Nanotechnology Perceptions
ISSN 1660-6795
www.nano-ntp.com

Simulation of the Collapse of a White Dwarf: A Didactic Proposal Using Spreadsheets

Brexys Linares Rodríguez[1], Manuel Alvarez Alvarado[2], Ulbio Durán Pico[1]

[1]Universidad Técnica De Manabí, Portoviejo-Ecuador
[2]Escuela Politécnica Del Litoral, Guayaquil-Ecuador
Email: blinares9307@utm.edu.ec

The simulation of the collapse of a white dwarf star is presented in spreadsheets in order to show the potentialities of Excel in the teaching of physics. A nonlinear model is deduced that describes the changes in the mass and density of a star along its radius, solved numerically using the fourth-order Runge-Kutta method in Excel. The numerical calculation provides the size and mass of the star for a central density profile compared to units of radius and solar masses, observing that at high densities the star collapses at the Chandrasekhar Limit. Form controllers are integrated for parameter adjustment and dynamic graphics, making it easy to visualize stellar collapse. The simulation was implemented to a population of students of the Bachelor's Degree in Physics. The participants' level of perception and satisfaction with the resource was measured with a 12-question questionnaire on a Likert scale. The results indicate a high satisfaction and positive perception towards simulation, highlighting its effectiveness in teaching complex physics concepts. This proposal shows how Excel, a versatile and accessible tool, allows teachers and students to carry out simulations without the need for advanced programming, promoting confidence in the use of computer technologies.

Keywords: Physics teaching, white dwarf, simulation, stellar collapse, Excel.

1. Introduction

Computer simulations are computer programs designed to reproduce an everyday or natural phenomenon in a virtual environment. Given the complexity of the phenomenon, these usually start from idealized situations that are approaching reality and are used as a bridge for understanding it. Thus, in the teaching of physics, the use of simulations is becoming more and more common, even being considered as experimental activities (Andrés, 2021). In addition, they are an alternative that allows breaking with the traditional teaching scheme in theoretical classes and makes it possible to recreate complex, abstract or risky physical systems for reproduction in a physical laboratory (Raviolo, 2012; Eso et al., 2018).

On the other hand, the use of simulators has experienced a significant increase with the birth of online education as a result of the COVID-19 pandemic (Razzak & Uddin, 2023). However, its use by teachers and students presents certain barriers. One of these limitations lies in the use of a programming language, which can be a complex task for many. On the other hand, the need for computer-intensive equipment and the financial requirements associated with the acquisition of software licences represent another significant obstacle. However, these limitations can be overcome through the use of spreadsheets (Sabarudiin et al., 2024).

Spreadsheets are widely available tools on any computer and one of the most popular today is the Excel spreadsheet developed by Microsoft Inc. Unlike programming languages that are usually discontinued, Excel is constant over time, retaining its main characteristics throughout updates. In this way, both teachers and students are becoming increasingly familiar with this tool due to its accessibility and ease of carrying out simulations without the need to master a specific programming language (Raviolo, 2011; Uddin et al., 2023). In this order of ideas, the Excel spreadsheet allows difficult equations to be simulated in a simple way compared to common programming languages such as Python and JavaScript (Purnama et al., 2023). In addition, it is possible to recreate simulations with an appearance similar to those available on the internet, which allows corroborating the veracity of the simulation online and knowing the mathematical models that make it up (Raviolo et al., 2011). We can also affirm that it is an environment to carry out experimental data processing in a simple way that leads to verifying or comparing the theory with the experiment (Suárez & Tornaría, 2019). Similarly, it allows the design of user interface guides (GUIs) that are characterized by presenting hidden algebra step by step with content that goes hand in hand with mathematical operations and is not limited to presenting only the result of a calculation such as those available online (Gul & Tufail, 2024).

The benefits offered by the Excel spreadsheet for teaching physics are evident, which leads us to the purpose of this work, which is to use the spreadsheet to simulate a complex phenomenon such as the collapse of a white dwarf star and the Chandrasekhar limit. This work begins with the deduction of a static model of a relativistic simple white dwarf. Next, the numerical solution of the model by the fourth-order Runge-Kutta method (RK4) in spreadsheets and the use of form controllers for the simulation of the collapse of the star and the visualization of the Chandrasekhar limit are shown. The implementation of the simulation to a population of students of the Bachelor's Degree in Physics is described and, to analyze the perception and satisfaction of the participants, the application of a Likert attitude questionnaire. Finally, the results of the instrument are analyzed and the main conclusions are presented

2. THEORETICAL FRAMEWORK

The famous physicist Stephen Hawking, in his literary work "History of Time", defines the white dwarf as a "stable cold star, maintained by the repulsion due to the principle of exclusion between electrons" (Hawking, 1988). This definition offers an overview of white dwarfs and is part of the theoretical model that is presented below under the following considerations:

Ideal fluid at rest

It is assumed that the fluid that makes up the white dwarf is ideal and is in a state of rest. Along

these lines, for a dynamic fluid, the Navier-Stokes equation:

$$\frac{\partial^2\vec{v}}{\partial t^2} + (\vec{v}\cdot\vec{\nabla})\vec{v} = -\frac{1}{\rho}\vec{\nabla}P + \mu\vec{\nabla}^2\vec{v} + \vec{g} \quad (1)$$

(De Jesús Rubio et al., 2013). For an ideal, non-viscous, $\mu = 0$, resting fluid, the equation is simplified to:$\vec{v} = 0$

$$\frac{1}{\rho}\vec{\nabla}P = \vec{g} \quad (2)$$

being density, pressure and gravitational field. Now, applying the divergence operator in equation (2):$\rho P\vec{g}$

$$\vec{\nabla}\cdot\left(\frac{1}{\rho}\vec{\nabla}P\right) = \vec{\nabla}\cdot\vec{g} \quad (3)$$

or

$$\vec{\nabla}\cdot\left(\frac{1}{\rho}\vec{\nabla}P\right) = -4\pi G\rho \quad (4)$$

where the gravitational field has been rewritten as $\vec{g} = -\vec{\nabla}\Phi$, with the potential solution of the Poisson equation . Quantity is the universal gravitational constant. Equation (4) is known as the hydrostatic equilibrium equation$\Phi\Delta\Phi = 4\pi G\rho G = 6.67\times10^{-11}\,N\cdot m^2/kg^2$.

Perfect spherical geometry

It is postulated that the white dwarf has a perfect spherical geometry. In this context, it is convenient to write the differential operators of equation (4) in spherical coordinates, but before proceeding, from the vector identity $\vec{\nabla}\cdot(u\vec{A}) = u\vec{\nabla}\cdot\vec{A} + \vec{A}\cdot\vec{\nabla}u$ the equilibrium equation is rewritten as:

$$\frac{1}{\rho}\Delta P + \vec{\nabla}P\cdot\vec{\nabla}\left(\frac{1}{\rho}\right) = -4\pi G\rho \quad (5)$$

Figure 1 shows a spherical volume element of the fluid transversely. Under hydrostatic conditions, there is no variation in pressure and density along the tangential components; that is, each layer of the sphere constitutes a surface of constant pressure and density. In fact, the density and pressure depend only on the radial coordinate. Therefore, the Laplacian and scalar product of the gradients $\Delta p\vec{\nabla}P$ and are written as: $\vec{\nabla}\rho^{-1}$

$$\Delta P = \frac{1}{r^2}\frac{\partial}{\partial r}\left(r^2\frac{\partial P}{\partial r}\right) \quad ; \quad \vec{\nabla}P\cdot\vec{\nabla}\left(\frac{1}{\rho}\right) = \frac{\partial P}{\partial r}\frac{\partial}{\partial r}\left(\frac{1}{\rho}\right)$$

Substituting these expressions in equation (5) and simplifying, we get:

$$\frac{1}{r^2}\frac{d}{dr}\left(\frac{r^2}{\rho}\frac{dP}{dr}\right) = -4\pi G\rho \quad (6)$$

Figure 1. Cross-section of the star.

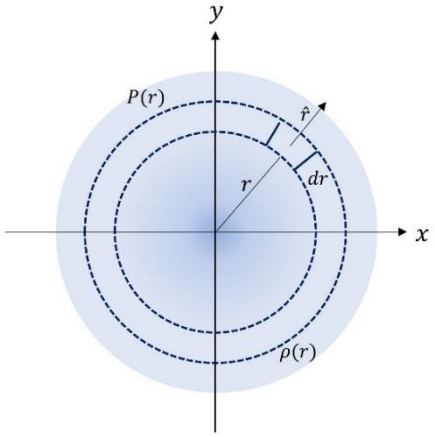

separating variables and given that for a spherical piece $\boldsymbol{dm = 4\pi\rho r^2 dr}$, it is detached:

$$\frac{d\rho}{dr} = -G\left(\frac{dP}{d\rho}\right)^{-1}\frac{m(r)\rho(r)}{r^2} \quad (7)$$

$$\frac{dm}{dr} = 4\pi\rho r^2 \quad (8)$$

In which . Note that the partial derivative has been rewritten as ordinary due to the exclusive dependence of the variables on the radial coordinate. The system of ordinary differential equations (7) and (8) provides a model of the mass and density of the star as a function of radius (Pei, 2022). The next step is to determine the relationship between pressure and density, for which thermodynamic principles and the following assumption will be used.$\boldsymbol{dP/dr = (d\rho/dr)(dP/d\rho)}$

Electrons as degenerate Fermi gas

The mass levels in a white dwarf are so high that gravity crushes the particles, confining the atomic nuclei inside, while the electrons, being the lightest particles, are overwhelmingly concentrated on the stellar surface. In this environment, the Pauli exclusion principle comes into play, manifesting itself as a

repulsion between identical fermions. This repulsion forces electrons to move at high speeds, close to that of light, in very small spaces, generating pressure

of electronic degeneracy that opposes the gravitational collapse of the star (Pinochet, 2019). As a result, the behavior of free electrons on the surface of the star is analogous to that of free electrons in a metal at absolute temperature, i.e., a relativistic degenerate Fermi gas$\boldsymbol{T \to 0}$.

To model this gas, we consider a large volume $\boldsymbol{V}$ containing electrons with energy. At the temperature limit, all states are occupied and all states are empty. Here, quantity is Fermi's

impulse. For this gas the average number and mean energy of electrons with states, degenerate gas, is calculated by the following equations: $\boldsymbol{N\varepsilon = \sqrt{c^2p^2 + (m_ec^2)^2}T \rightarrow 0p < p_Fp > p_Fp_F\bar{N}\bar{E}p < p_F}$

$$\bar{N} = 2V\int_0^{p_F}\frac{d^3p}{(2\pi\hbar)^3} \quad (9)$$

$$\bar{E} = 2V\int_0^{P_F}\frac{d^3p}{(2\pi\hbar)^3}\sqrt{c^2p^2 + (m_ec^2)^2} \quad (10)$$

where the speed of light, $\boldsymbol{c = 3\times10^8\, m/s}$ $\hbar = \mathbf{1.05\times10^{-34}J\cdot s}$ Planck's constant is reduced and is the mass of the electron. By integrating equations (9) and (10) in the phase space in spherical coordinates, we obtain: $\boldsymbol{m_e = 9.1\times10^{-31}kgd^3p = 4\pi p^2dp}$,

$$p_F = \hbar\left(3\pi^2n\right)^{1/3} \quad (11)$$

$$\bar{E} = n_0m_ec^2Vx^3\epsilon(x) \quad (12)$$

where $\boldsymbol{n = N/V}$ the concentration of electrons and the parameters and defined as:$\boldsymbol{x\epsilon(x)}$

$$\epsilon(x) = \frac{3}{8x^3}\left[x\left(2x^2+1\right)\sqrt{x^2+1} - ln\left[x+\sqrt{x^2+1}\right]\right] \quad (13)$$

$$x \equiv \frac{p_F}{m_ec} = \left(\frac{n}{n_0}\right)^{1/3} = \left(\frac{\rho}{\rho_0}\right)^{1/3} = \left(\frac{N}{\rho_0V}\right)^{1/3} \quad (14)$$

The quantity $\boldsymbol{n_0 = m^3c^3/\left(3\pi^2\hbar^3\right) = 5.85\times10^{35}m^{-3}}$ is the Fermi density and the parameter characterizes the relative electron density. It is notable that $\boldsymbol{xx}$ it also relates to the relative mass density, since, for a given amount of mass, the electron concentration is , being the number of free electrons per nucleon and is the mass of the proton. In addition, it has to be the mass density of matter where the electron density is $\boldsymbol{n = Y_e\rho/M_pY_eM_p = 1.67\times10^{-27}kg\rho_0 = M_pn_0Y_e^{-1} = 9.78\times10^8Y_e^{-1}\,kg/m^3\,n_0}$(Koonin & Meredith, 1990).

The purpose of calculating the average energy of the electronic gas lies in the determination of the gas pressure, which is obtained from the derivative of the average energy with respect to volume (Pei, 2023), as indicated in equation (14)

$$P = -\frac{\partial\bar{E}}{\partial V} \quad (15)$$

This expression is derived from the first law of thermodynamics, considering the temperature limit, where entropy is a constant according to the third principle of thermodynamics. Thus, calculating in equation 12, equation 14 and using partial differential properties in equation 15, we obtain: $\boldsymbol{d\bar{E} = TdS - PdVT \rightarrow 0S\partial_\epsilon\bar{E} = n_0m_ec^2Vx^3\partial_Vx = -x/3V}$

$$\begin{aligned} \boldsymbol{P} &= -\frac{\boldsymbol{\partial \bar{E}}}{\boldsymbol{\partial \epsilon}} \cdot \frac{\boldsymbol{\partial x}}{\boldsymbol{\partial V}} \cdot \frac{\boldsymbol{\partial \epsilon}}{\boldsymbol{\partial x}} \\ &= -\left(\boldsymbol{n_0 m_e c^2 V x^3}\right)\left(-\frac{\boldsymbol{x}}{\boldsymbol{3V}}\right)\frac{\boldsymbol{\partial \epsilon}}{\boldsymbol{\partial x}} \\ &= \frac{\boldsymbol{1}}{\boldsymbol{3}}\boldsymbol{n_0 m_e c^2 V x^4 \epsilon'(x)} \end{aligned} \tag{16}$$

Now, calculating $\boldsymbol{dx/d\rho = 1/\left(3x^2\rho_0\right)}$ in equation 14, deriving equation 16 with respect to pressure and applying properties of ordinary derivatives, we have

$$\begin{aligned} \boldsymbol{P} &= -\frac{\boldsymbol{\partial P}}{\boldsymbol{\partial x}} \cdot \frac{\boldsymbol{\partial x}}{\boldsymbol{\partial \rho}} \\ &= \left(\frac{\boldsymbol{1}}{\boldsymbol{3x^2\rho_0}}\right)\frac{\boldsymbol{d}}{\boldsymbol{dx}}\left[\frac{\boldsymbol{1}}{\boldsymbol{3}}\boldsymbol{n_0 m_e c^2 V x^4 \epsilon'(x)}\right] \\ &= \frac{\boldsymbol{n_0 m_e c^2}}{\boldsymbol{3\rho_0}}\frac{\boldsymbol{1}}{\boldsymbol{9x^2}}\frac{\boldsymbol{d}}{\boldsymbol{dx}}\boldsymbol{[x^4 \epsilon'(x)]} \end{aligned} \tag{17}$$

Since:

$$\frac{\boldsymbol{1}}{\boldsymbol{9x^2}}\frac{\boldsymbol{d}}{\boldsymbol{dx}}\boldsymbol{[x^4 \epsilon'(x)]} = \frac{\boldsymbol{x^2}}{\boldsymbol{3\sqrt{1+x^2}}}$$

The result is simplified as:

$$\boldsymbol{P} = \frac{\boldsymbol{n_0 m_e c^2}}{\boldsymbol{3\rho_0}}\frac{\boldsymbol{x^2}}{\boldsymbol{\sqrt{1+x^2}}} \tag{18}$$

Equation 18 provides the variation of pressure with density given that it is the relative mass density. Substituting equation 16 into equation 7 yields:$\boldsymbol{x}$

$$\frac{\boldsymbol{d\rho}}{\boldsymbol{dr}} = -\frac{\boldsymbol{3G\rho_0}}{\boldsymbol{n_0 m_e c^2}}\frac{\boldsymbol{\sqrt{1+x^2}}}{\boldsymbol{x^2}}\frac{\boldsymbol{m(r)\rho(r)}}{\boldsymbol{r^2}} \tag{19}$$

$$\frac{\boldsymbol{dm}}{\boldsymbol{dr}} = \boldsymbol{4\pi\rho r^2} \tag{20}$$

Note that the presence of the variables $\boldsymbol{m(r)}$ y in equation 17 makes the system of equations a nonlinear system, so its solution must be numerical. However, the stability of the numerical method may be affected because the value of the coefficient in equation 17 is of the order . For this reason, it is advisable to work as much as possible with quantities of an order of magnitude close to unity. For this reason, it is convenient to rewrite the radius, mass, and density as: $\boldsymbol{\rho(r) \sim 10^{-24}}$

$$\boldsymbol{r = R_0 \bar{r}} \quad , \quad \boldsymbol{m = M_0 \bar{m}} \quad , \quad \boldsymbol{\rho = \rho_0 \bar{\rho}} \tag{19}$$

where $\boldsymbol{\bar{r}}$, $\boldsymbol{\bar{m}}$ and dimensionless quantities and $\boldsymbol{\bar{\rho} R_0}$, $\boldsymbol{M_0}$ and scales of radius, mass, and density respectively. Replacing (19) in (17) and (18) gives you:$\boldsymbol{\rho_0}$

$$\frac{d\bar{\rho}}{d\bar{r}} = -\left(\frac{G\rho_0 M_0}{n_0 m_e c^2 R_0}\right)\frac{3\sqrt{1+\bar{\rho}^{2/3}}}{\bar{\rho}^{2/3}}\frac{\bar{m}\bar{\rho}}{\bar{r}^2}$$

$$\frac{dm}{dr} = \left(\frac{4\pi R_0^3 \rho_0}{M_0}\right)\bar{\rho}\bar{r}^2$$

Y scales $\boldsymbol{R_0}$ are defined in such a way that the coefficients in parentheses are equal to unity:$\boldsymbol{M_0}$

$$R_0 \equiv \sqrt{\frac{Y_e m_e c^2}{4\pi G \rho_0 m_p}} = 7.76 \times 10^6 m Y_e \quad , \qquad M_0 = 4\pi\rho_0 R_0^3 = 5.67 \times 10^{30} kg\, Y_e^2 \tag{20}$$

Therefore, the following system of dimensionless differential equations is obtained:

$$\frac{d\bar{\rho}}{d\bar{r}} = -\frac{3\sqrt{1+\bar{\rho}^{2/3}}}{\bar{\rho}^{2/3}}\frac{\bar{m}\bar{\rho}}{\bar{r}^2} \tag{21}$$

$$\frac{d\bar{m}}{d\bar{r}} = \bar{\rho}\bar{r}^2 \tag{22}$$

The numerical solution of the previous system requires the fixing of the initial or boundary conditions. However, because the system is unique in $\bar{r} = 0$, it is not possible to freely establish such conditions. In this context, it is appropriate to discuss the properties that are expected for the system. First, the existence of two distinct regions is anticipated: a region of matter, corresponding to the star, and a region of vacuum on the outside. The place where it passes from one situation to another defines the dimensionless radius of the star $\bar{R}$ (Aceña, 2020). The dimensionless mass contained in the star is expressed as . In regions outside the star (, you have to and . On the other hand, in the interior of the star, it is positive and monotonically decreasing, while it is positive and monotonically increasing. The integration domain ranges from to . However, since the value of is initially unknown, the only viable option is to set initial conditions in the vicinity of . Therefore, the initial conditions for the system in terms of mass and density are:$\bar{M} = \bar{m}(\bar{R})\bar{r} \geq \bar{R})\bar{\rho} = 0\bar{m} = M(r < R)\bar{\rho}\bar{m}\bar{r} = 0\bar{r} = \bar{R}\bar{R}\bar{r} = 0$

$$\bar{m}(0) = 0 \quad , \qquad \bar{\rho}(0) = \rho_c \tag{23}$$

The choice of is based on the premise that the center of the star has no initially accumulated mass, and the accretion begins as we move away from the center. Regarding density, it is emphasized that the presence of the radical in equation (21) implies that it must be positive and finite for the system to be regular. The value of is the central density.$\bar{m}(0) = 0\bar{\rho}\rho_c$

The numerical solution of the initial value problem (21), (22), and (23) together with the scalable quantities (20) and (20), provides a model that describes how the mass and density of the star change as we move away from the center. The solution is determined by the numeric value that is chosen. Since the vast majority of white dwarfs are composed primarily of Y_e [12C,](#) it is selected $Y_e = 0.5$ for this element. In addition, it is interesting to express the results with the solar units of mass and radius

$$\boldsymbol{R_{\odot} = 6.96 \times 10^{8} m} \ , \qquad \boldsymbol{M_{\odot} = 1.99 \times 10^{30} kg} \qquad (24)$$

and with the density at the center of the sun, approximately . When comparing the radio and mass scales at (20) with solar units (24), white dwarf stars are expected to have masses comparable to solar mass, but with considerably smaller radii and much higher densities. $\boldsymbol{1.5 \times 10^{5}\, kg/m^{3}}$Solutions for central density profiles $\boldsymbol{\rho_c}$ in the range of $\boldsymbol{10^{n-3}}$. For numerical integration, the RK4 method will be used due to its effectiveness, see Appendix. However, it is crucial to point out that the RK4 method will not work if we try to integrate exactly from $\boldsymbol{n = 1..12\bar{r} = 0}$ because it is a singular point in the equation (21). Instead, we'll move the initial conditions to a later point, conveniently chosen as . The details of implementing the RK4 method in a spreadsheet are described in the next section$\boldsymbol{\bar{r} = 10^{-20}}$

3. METHODOLOGY

We proceed to describe the simulation of the mass-radius relationship of the model described in the previous section in spreadsheets.

Numerical solver: RK4 method in spreadsheets

To numerically solve PVI 21, 22 and 23, a numerical solver is developed in an Excel spreadsheet. Figure 2 provides a detailed visualization of this numerical solver, which requires the specification of the center density (cell P4) and radius (cell V4) as input data. As a result, a matrix with the numerical solution of the problem. The initial values for radius, density and mass are set in cells B7, K7 and L7 respectively. The formulas of the RK4 numerical method are then inserted into the B8:L8 cell range.

Figure 2. Numerical solver in spreadsheet

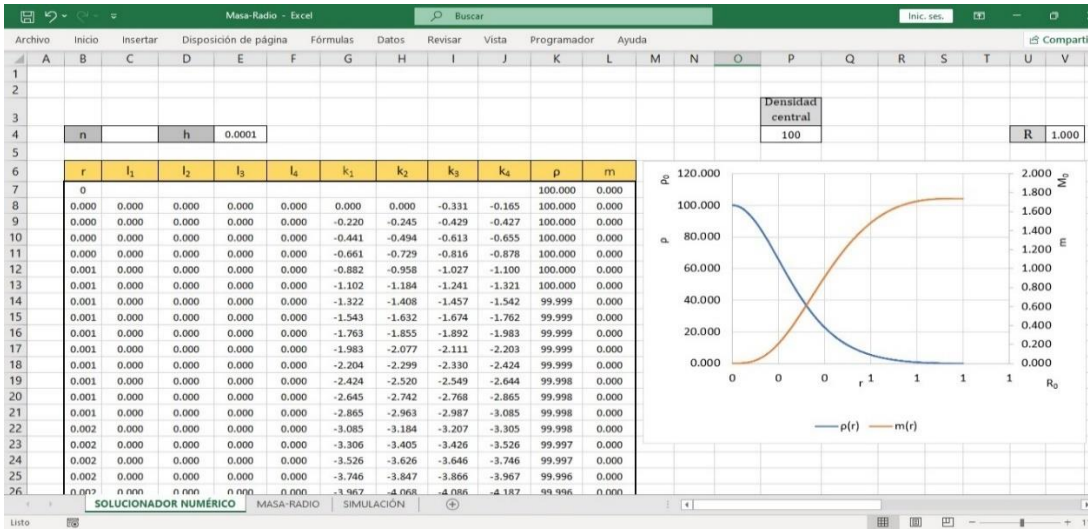

Table 1 presents the formulas used, as well as the variables they represent. It should be noted that the values displayed from row 9 onwards are generated by replicating the formulas in row 8 by dragging the fill handle to subsequent rows. Indeed, the data in columns B, K, and L

starting from row 7 represent the numerical solution to the problem.

Table 1. Numerical solver formulas in worksheet

Column/Cell	Variable	Description	Worksheet Command
E4	$\boldsymbol{h}$	Step	=0.0001
Q4	$\boldsymbol{\rho_c}$	Core density	=100
V4	$\boldsymbol{R}$	End radius	=1
B7	$\bar{\boldsymbol{r}}_{\boldsymbol{0}}$	Initial radius	=10^(-19)
K7	$\bar{\boldsymbol{\rho}}(\boldsymbol{0})$	Core density	=N4
L7	$\bar{\boldsymbol{m}}(\boldsymbol{0})$	Central mass	=0
B8	$\bar{\boldsymbol{r}}$	Radio	=B7+$E$4
C8	$\boldsymbol{l_1}$	Coefficient $\boldsymbol{l_1}$	=K7*B7^2
D8	$\boldsymbol{l_2}$	Coefficient $\boldsymbol{l_2}$	=(K7+0.5*G8*$E$4)*(B7+0.5*$E$4)^2
E8	$\boldsymbol{l_3}$	Coefficient $\boldsymbol{l_3}$	=(K7+0.5*H8*$E$4)*(B7+0.5*$E$4)^2
F8	$\boldsymbol{l_4}$	Coefficient $\boldsymbol{l_4}$	=(K7+I8*$E$4)*(B7+$E$4)^2
G8	$\boldsymbol{l_1}$	Coefficient $\boldsymbol{k_1}$	=-3*ROOT((K7^2)^(1/3)+1)*L7*K7^(1/3)/B7^2
H8	$\boldsymbol{l_2}$	Coefficient $\boldsymbol{k_2}$	=-3*ROOT((((K7+0.5*G8*$E$4)^2)^(1/3)+1)*(L7+0.5*C8*$E$4) *(K7+0.5*G8*$E$4)^(1/3)/(B7+0.5*$E$4)^2
I8	$\boldsymbol{l_3}$	Coefficient $\boldsymbol{k_3}$	=-3*ROOT((((K7+0.5*H8*$E$4)^2)^(1/3)+1)*(L7+0.5*D8*$E$4) *(K7+0.5*H8*$E$4)^(1/3)/(B7+0.5*$E$4)^2
P8	$\boldsymbol{l_4}$	Coefficient $\boldsymbol{k_4}$	=-3*ROOT(((K7+I8*$E$4)^2)^(1/3)+1)*(L7+E8*$E$4) *(K7+I8*$E$4)^(1/3)/(B7+$E$4)^2
K8	$\bar{\boldsymbol{\rho}}(\bar{\boldsymbol{r}})$	Density	=K7+$E$4*(G8+2*H8+2*I8+J8)/6
L8	$\bar{\boldsymbol{m}}(\bar{\boldsymbol{r}})$	Mass	=L7+$E$4*(C8+2*D8+2*E8+F8)/6

The graphical representation of these results (see Figure 2) is presented in a scatterplot of smoothed lines. This graph provides a clear visualization of the change in mass and density along the radius in response to the specified initial conditions.

Estimation of the Radius and Mass of the Star: Chandrasekhar Limit

The results provided by the numerical solver are consistent with what is expected: regardless of the value assigned to the central density (cell P4), as it is numerically integrated for values far from the center of the star, the density decreases with an asymptotic behavior to zero, and the mass increases with an asymptotic behavior towards the maximum value. The bounded value of the radius is entered in cell V4. Now, through solver we proceed to estimate the mass and size defined by the star for a specific value of the central density. As discussed above, these values are initially unknown. $\bar{\boldsymbol{M}}\bar{\boldsymbol{R}}\bar{\boldsymbol{\rho}}_{\boldsymbol{c}}$

To determine the total mass of the star and its size, solutions for a density profile of con , using a step size of . The maximum values of radius and mass are selected where the ratio $\boldsymbol{10^{n-3}n = 1..1210^{-3}\bar{\rho}(R)/\bar{\rho}_c \sim 10^{-6}}$. That is, an edge is chosen where the density is significantly lower compared to the central density. Figure 3 shows the maximum mass and radius values (dimensionless) that the star reaches for the aforementioned density profile. Likewise, the equivalent of the mass and radius of the sun is shown, along with the percentage of reduction

of the radius with increasing central density (cell range AI10:AN21).

Figure 3. Radius and mass of the star in solar units

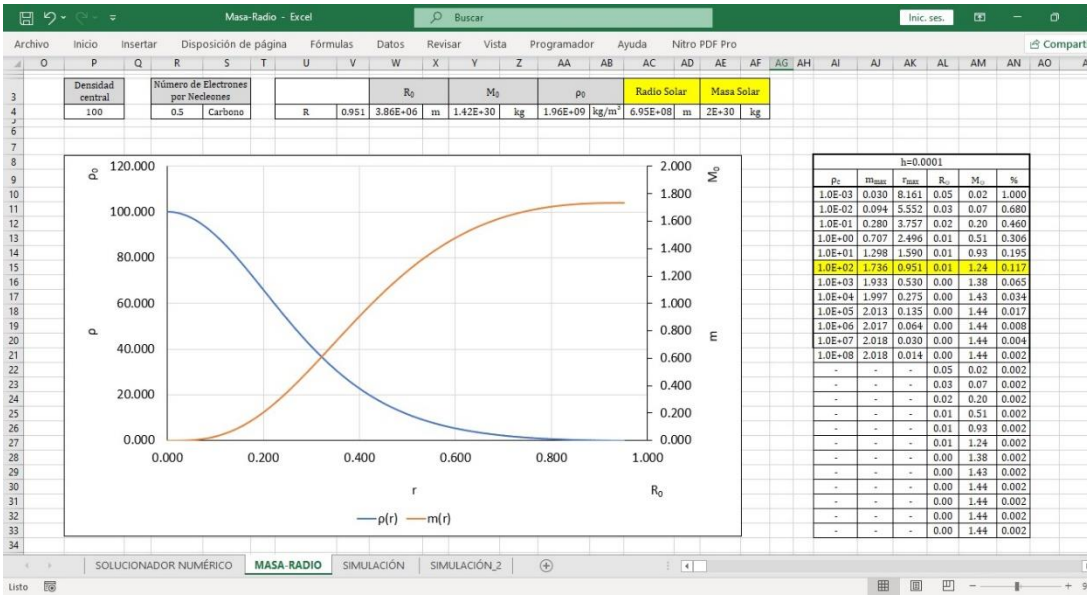

Table 2 shows the formulas used and the associated variables for the scales. It is important to note that, for high density values, the size of the star decreases considerably. Compared to the solar radius scale, the radius tends to zero, reaching the collapse situation, and the mass tends to $\mathbf{1.44}\,\boldsymbol{M_{\odot}}$. This value is known in the literature as the Chandrasekhar limit and corresponds to the maximum stable mass of a white dwarf star (Pinochet, 2020; Low, 2023). Figure 3 additionally shows, for comparison purposes, that along the range of cells R4:AF4 the values of the constant$\boldsymbol{Y_e}$, the scales of radius, mass and density, as well as the units of radius and solar mass are entered.

Table 2. Spreadsheet formulas for mass and radius scales

Column/Cell	Variable	Description	Worksheet Command
AL10	$\boldsymbol{R_{\odot}}$	Solar Radio Scale Quantity	=AK10*$W$4/$AC$4
AM10	$\boldsymbol{M_{\odot}}$	Quantity in solar mass scale	=AJ10*$Y$4/$AE$4
AN10	%	Radius reduction	=AL10/$AL$10
Q4	$\boldsymbol{Y_e}$	Number of electrons per nucleon	=0.5
W4	$\boldsymbol{R_o}$	Radio Scale	=7.72*10^6*R4
Y4	$\boldsymbol{M_o}$	Mass Scale	=5.67*10^30*R4^2
AA4	$\boldsymbol{\rho_o}$	Density Scale	=9.78*10^8*R4^(-1)
AC4	Radio Solar	Sun Radio	=6.95*10^8
AE4	Solar Mass	Mass of the Sun	=1.98*10^30

Note that in the AL22:AN33 cell range, solar mass values, solar radius and percentage of radius reduction are repeated. These data will be used for the simulation of the mass-radius relationship, as described in the next section.

Programmer Elements: Star Collapse Simulation

Once the numerical solutions have been obtained, arrays and programmer elements of the spreadsheet are incorporated to visualize the behavior of the model when adjusting the parameters. As for arrays, in cell C4 the number of partitions used in the numerical solution is entered, which requires setting a finite number of points. This implies that the value of the step in cell E4 must be modified, as detailed in Table 3.

Figure 4 illustrates the incorporation of programmer elements. First, a numerical controller linked to cell AL4 is assigned for density profile adjustment. The values it takes when you press the button correspond to those of the AI10:AI21 range matrix. A scroll bar linked to the AK4 cell is then assigned for the radius, taking values from zero to the maximum value of the radius associated with the set density profile. Table 3 shows how the incorporation of these programming elements leads to the modification of the formulas in cells P4 and V4. Likewise, Figure 4 shows that the values in the range of cells B7:B1007, K7; K1007 and L7:L1007 are initially used to produce a scatterplot of smoothed lines that simultaneously shows the change in mass and density along the radius. However, in order to have the freedom to display the change in mass or density individually, a checkbox control linked to cell AJ5 is assigned for mass values and another checkbox control linked to cell AL5 for density values. Because the checkbox controls work with logical statements, the density and mass values represented in the cell range K7:K1007 and L7:L1007 are no longer considered for the graph. Instead, the mass and density values are reprogrammed along the range of N7:N1007 and M7:M1007 cells respectively. Table III shows the formulas used for the reprogramming of the mass and density values in the new matrices.

Table 3. Reprogramming Formulas by Using Scheduler Controls

Column/Cell	Variable	Description	Worksheet Command
C4	$\boldsymbol{n}$	Number of partitions	=1000
E4	h	step	=V4/C4
Q4	$\boldsymbol{\rho_c}$	Core density	=INDEX(AI10:AK21; AI4; 1)
V4	$\boldsymbol{R}$	End radius	=AK4*AJ4*0.001
M4	$\bar{\boldsymbol{\rho}}(\bar{\boldsymbol{r}})$	Density as a function of radius	=IF($AI$5=TRUE; K7;-1)
N4	$\bar{\boldsymbol{m}}(\bar{\boldsymbol{r}})$	Mass as a function of radius	=IF($AJ$5=TRUE; L7;-1)
P27	$\bar{\boldsymbol{r}}$	Local Radio	=INDEX(B7:N1007; AL4; 1)
R27	$\bar{\boldsymbol{\rho}}$	Local density	=INDEX(B7:N1007; AL4; 12)
S27	$\bar{\boldsymbol{m}}$	Local dough	=INDEX(B7:N1007; AL4; 13)
Y27	$\boldsymbol{\rho}$	Central density of the star	=INDEX(AI10:AN21; AM4; 1)*AA4
AA27	$\boldsymbol{M}$	Mass of the star in units $\boldsymbol{M}_{\odot}$	=INDEX(AI10:AN21; AM4; 5)
AC27	$\boldsymbol{R}$	Star radius in units $\boldsymbol{R}_{\odot}$	=INDEX(AI10:AN21; AM4; 4)
AE27	%	Radius reduction percentage	=INDEX(AI10:AN21; AM4; 6)

On the other hand, at the bottom of the graph, along the P27:U27 cell range, the point values mass and density are programmed for a given radius. These three values are assigned two numerical controls linked to cell AL4. The difference between the two controls is that one has higher magnification. These point values are represented by a scatter plot, combined with the smoothed line scatter plot of the range matrices B7:B1007, N7; N1007 and M7:M1007, resulting in two points that can slide along curves.

Figure 4: Programmer Elements for Parameter Adjustment

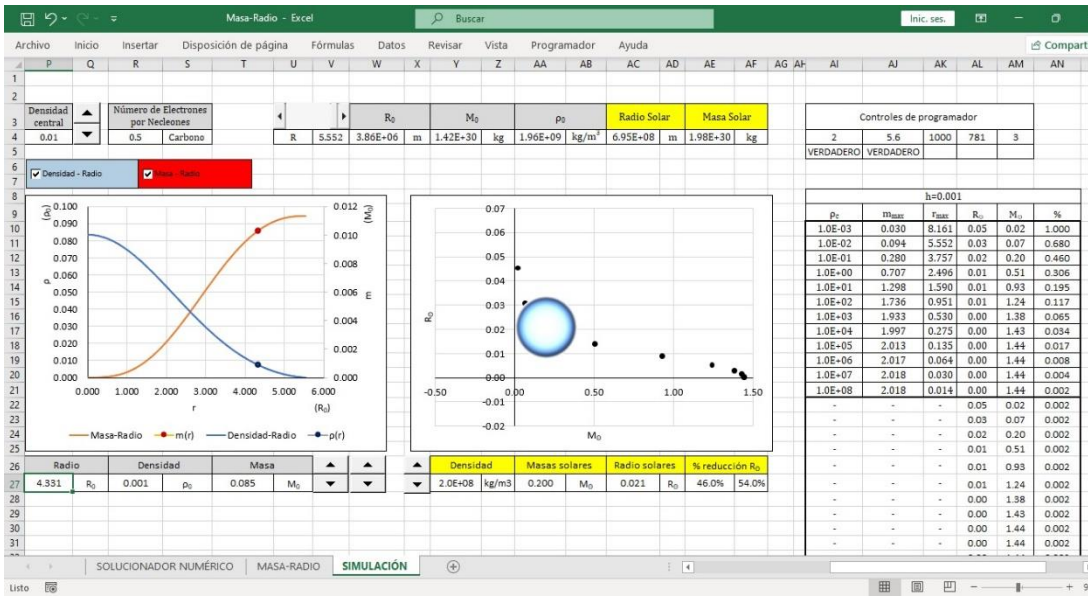

However, the values shown in the cell range AL10:AN33 are used to graph the mass-radius ratio and simulate the collapse of the star as it approaches the Chandrasekhar limit limit. To carry out the simulation, the combination of three bubble charts is used. The first graph is made with the values of the cell range AL22:AN33, with the aim that the bubbles have the same size and leave the trace of a dot plot. The second graph is made with the AL10:AN33 cell range to visualize the decrease in the size of the star as its mass increases. The design of this graphic is such that it has an unfilled and outline-free background. The last graph is made with the combination of numerical values of the cell range Y27:AF27, which represent the point values of solar mass, solar radius and percentage reduction of the star for a specific density value in the already established range. As this graph generates a single bubble, a white dwarf image is inserted into it for a greater didactic illustration of the phenomenon. The point values are assigned a numerical control linked to cell AM6 so that, when the button is pressed, it can be seen how the density increases, the size of the star decreases and its mass increases, reaching the situation of collapse at the Chandrasekhar limit.

Figure 5 shows only the slice of the spreadsheet that contains the numeric controls and charts, where the user adjusts the input parameters and looks at the results on the chart with point values and the simulation. The definition of the work sector was made with the option to hide in the spreadsheet. The following section describes the methodology to know what attitude students have towards the implementation of this simulation of the structures of white dwarfs and stellar collapse in the Excel spreadsheet.

Figure 5. Simulating the mass-radius ratio of a white dwarf in spreadsheet

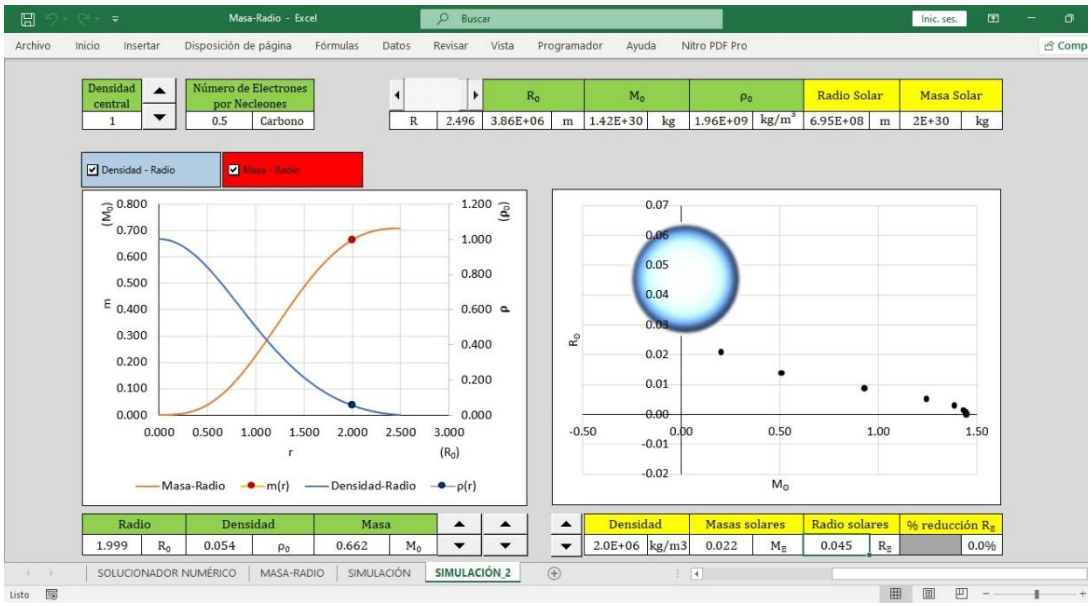

Level of perception and satisfaction of the simulation in Excel

An online webinar was held for students of the Bachelor's Degree in Physics attached to the Dean of Science and Technology of the Universidad Centroccidental Lisandro Alvarado (UCLA-DCyT), Venezuela. The webinar, entitled "White Dwarfs and Collapse at the Chandrasekhar Limit", was addressed in an informative and sequential manner, presented in three blocks: theoretical model, numerical treatment of the model in spreadsheet, and the results presented directly from the simulation, as shown in Fig. 5. In addition to the physical findings provided by the model, much emphasis was placed on the ease and benefits of the Excel spreadsheet to address complex physics problems.

To estimate the level of perception and satisfaction with the simulation in Excel, a questionnaire with 12 questions was implemented online using a 5-point Likert attitude scale. The global instrument was divided into 6 aspects that seek to inquire into the participants:

- Introduction and context: Familiarization and pre-webinar experience with the topic of white dwarfs and the use of Excel in educational activities.

- Experience during the talk: Qualification of the presentation through simulation and explanation of the theoretical model and methodology in the simulation.

- Use and understanding of the simulation: Perception of the simulation of the collapse of the star in Excel and improvement in the understanding of white dwarfs and stellar collapse.

- Interactivity and learning tools: Feedback on the effectiveness of the charts, visualization of the results, and ability to interact with the simulation using the form controls.

- Practical application and learning: Consideration of the use of simulations to improve physics teaching and motivation to discuss the collapse of white stars after the webinar.

- Overall satisfaction: Rating of the talk and simulation, and recommendation of simulation for physics teaching.

The statistical treatment of the survey results was carried out using the specialized software Statistical Product and Service Solutions (SPSS) and the Excel spreadsheet. To measure the reliability of participants' responses, Cronbach's alpha was used (Watson et al., 2023 ; Giday & Perumal, 2024). Table 4 shows the weighting of the index, which indicates the internal consistency and validity of the collection instrument. To analyze perception and satisfaction, a combined bar graph of percentages was used, distributed in the dimensions of very high, high, moderate, low and very low [18].

4. RESULTS

The results of the statistical treatment of the surveys are presented. Table 4 shows that Cronbach's alpha coefficient was 0.82, indicating a "Good" level of reliability. This suggests that the instrument is reliable and that the survey questions are consistent with each other, with consistent responses from participants.

Table 4. Reliability Statistics

Cronbach's alpha	N of elements	Weighting (Cronbach's alpha coefficient)	Magnitude
0.82	12	0.91 to 1.00	Excellent
		0.81 to 0.90	Well
		0.71 to 0.80	Acceptable
		0.61 to 0.70	Questionable
		0.51 to 0.60	Poor
		< 0.5	Unacceptable

Figure 6 shows that, of the P1 and P2 questions in the introduction and context category, it was observed that 11.5% of the participants rated their familiarity with the topic of white dwarfs as "Very High", while 53.8% rated it as "Moderate" and 34.6% as "Low". As for their previous experience with Excel in educational activities, 15.4% of participants rated it as "High," 46.2% as "Moderate," 34.6% as "Low," and 3.8% as "Very Low."

Regarding questions P3 and P4, experience during the talk, the clarity of the presentation was considered "Very High" by 57.7% of the participants and "High" by 42.3%. The usefulness of the examples and explanations was rated as "Very High" by 46.2% and "High" by 53.8%.

Regarding the use and understanding of the simulation, questions P5 and P6, 23.1% of the participants indicated that the ease of understanding and following the simulation with Excel is "Very High", 42.3% rated it as "High", 30.8% as "Moderate" and 3.8% as "Low". In addition, 53.8% of participants "Strongly Agree" that the simulation helped improve understanding of white dwarfs and stellar collapse, while 38.5% "Agree."

Figure 6. Simulation Perception and Satisfaction Statistics . In original language Spanish

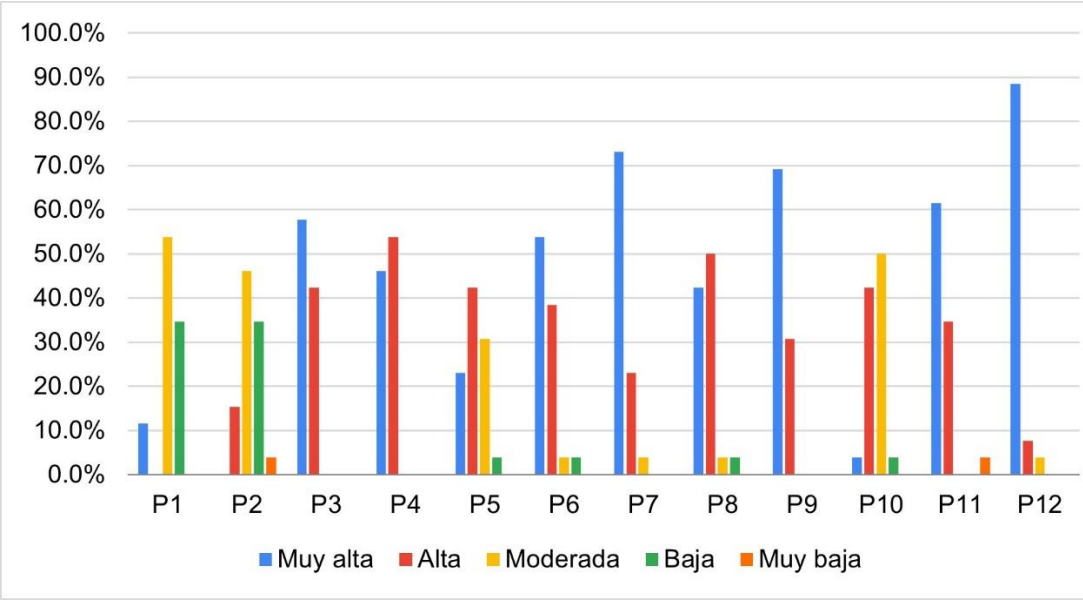

For questions P7 and P8, which address interactivity and learning tools, the effectiveness of the graphs and visualizations was rated as "Very High" by 73.1% of participants and "High" by 23.1%. The ability to interact with the simulation using the form controls was rated as "Very High" by 42.3%, "High" by 50.0%, and "Moderate" by 3.8%.

In terms of practical application and learning, reflected in questions P9 and P10, 69.2% of participants "Strongly Agree" that simulations are useful for improving physics teaching, while 30.8% "Agree". As for the motivation to discuss star collapse after the webinar, 3.8% rated it as "Very High," 42.3% as "High," and 50.0% as "Moderate."

Finally, in the general satisfaction section, questions P11 and P12, 61.5% of participants rated their overall satisfaction with the talk and simulation as "Very High" and 34.6% as "High". In addition, 88.5% of participants "strongly agree" in recommending this simulation for physics teaching, while 7.7% "Agree."

The favorable attitude on the part of the students towards the resource is notorious. A high percentage recognize the ease of Excel to understand and follow the simulation. They also agreed that the simulation helped improve understanding of white dwarfs and stellar collapse. Respondents' perceptions of Excel's effectiveness in visualizing and presenting graphs, as well as the ability to interact with the simulation using form controls, are highly positive. The vast majority consider that simulations improve the teaching and learning of complex physics concepts. The positive satisfaction of the resource is reflected in the high percentage of participants who would recommend the simulation addresses to other students or colleagues interested in teaching physics

5. CONCLUSIONS

The study demonstrates how the Excel spreadsheet can be used for physics teaching, specifically in the simulation of phenomena modeled by differential equations, such as the structures and collapse of white dwarf stars. Thanks to the layout of cells in the spreadsheets, the ease of inserting formulas and the dragging option, it is possible to work with the RK4 method in an orderly, friendly and illustrative way. This methodology facilitates the approach to the numerical solution of the model. The physical findings of the solution can be visualized in a didactic manner using smoothed line scatter charts, animated by form controls. In the model presented, the size of the star is determined from the asymptotic behavior of mass and density, regardless of the central density value set. It is observed that, by ordering the dimensions of the star in units of mass and solar radius, at high densities, the mass of the star is concentrated in a very small region, collapsing at the Chandrasekhar limit. The dynamic collapse simulation is executed by bubble graphs representing the mass-radius ratio, animated by a numerical control. Visualizing the phenomenon is crucial for understanding the physical processes that govern the death of stars.

Presenting this type of simulations in the classroom allows the teacher to break with traditional teaching schemes, which are often based on the explanation of complex phenomena or the development of theories on the blackboard, which can be monotonous and exhausting for students. On the other hand, simulations provide students with the opportunity to visualize and understand the phenomenon interactively, broadening their horizon to appreciate the beauty of the mathematical formalism used to model the event. The simplicity of the proposal shows how the Excel spreadsheet, an accessible and versatile tool, is an environment in which teachers and students can carry out programming tasks in a friendly way, without the need to master a specific language, which enhances creativity and confidence in the use of computer technologies. This environment not only opens up a world of possibilities for problem solving in physics, but also encourages exploration, promotes active learning and discovery in the educational process. Finally, it is highlighted that the simulation developed in this work can be used in courses of astronomy, astrophysics, numerical methods of physics and differential equations in physics.

References

1. Aceña, A. E. (2020). A very simple star. Revista Brasileira de Ensino de Física, 42. https://doi.org/10.1590/1806-9126-rbef-2020-0332
2. Andrés, M. M. (2021). Online experimental problem situations for learning physics. Journal of Physics Education, 33(2), 45–53. https://doi.org/10.55767/2451.6007.v33.n2.35168
3. De Jesús Rubio, J., Ordaz, G., Jiménez-Lizárraga, M., & Cabrera, R. I. (2013). General solution of the Navier–Stokes equation to describe the dynamics of a homogeneous viscous fluid in an open pipe. Revista Mexicana de Física, 59(3), 217-223. https://dialnet.unirioja.es/servlet/articulo?codigo=4418554
4. Eso, R., Safiuddin, L. O., Agusu, L., & Arfa, L. M. R. F. (2018). Simulation of 2D Waves in Circular Membrane Using Excel Spreadsheet with Visual Basic for Teaching Activity. Journal Of Physics Conference Series, 1011, 012088. https://doi.org/10.1088/1742-6596/1011/1/012088
5. Giday, D. G., & Perumal, E. (2024). Students' perception of attending online learning sessions

post-pandemic. Social Sciences & Humanities Open, 9, 100755. https://doi.org/10.1016/j.ssaho.2023.100755
6. Gul, S., & Tufail, M. Y. (2024). GUI for conic sections: parabola, ellipse and hyperbola. Revista Mexicana de Física E, 21(1), 1-5. https://doi.org/10.31349/revmexfise.21.010203
7. Hawking, S. (1989). A brief history of time: From the big bang to black holes. Prentice Hall & IBD
8. Koonin, S. E., & Meredith, D. (1990). Computational physics: Fortran version. Westwiew Press
9. Low, A. M. (2023). The Chandrasekhar limit: a simplified approach. Physics Education, 58(4), 045008. https://doi.org/10.1088/1361-6552/acdbb0
10. Pei, T. (2022). The Highly Accurate Relation Between the Radius and Mass of the White Dwarf Star From Zero to Finite Temperature. Frontiers In Astronomy And Space Sciences, 8. https://doi.org/10.3389/fspas.2021.799210
11. Pei, T. (2023). The additional pressure of white dwarf stars generated by net charges. Publications Of The Astronomical Society Of Japan, 75(5), 893-906. https://doi.org/10.1093/pasj/psad047
12. Pinochet, J. (2020). The Chandrasekhar limit for beginners. Revista Mexicana de Física E, 17(2), 125-132. https://doi.org/10.31349/revmexfise.17.125
13. Pinochet, J. (2019). Brown dwarfs and the minimum mass of stars. Physics Education, 54(5), 055021. https://doi.org/10.1088/1361-6552/ab2b15
14. Purnama, A. Y., Ariswan, N., Istiyono, E., Putranta, H., Rani, S. A., Wijayanti, A., & Saputri, R. (2023). Particle trajectory simulation using python and spreadsheet as an online learning alternative. Revista Mexicana de Física E, 20(2), 1-6. https://doi.org/10.31349/revmexfise.20.020202
15. Raviolo, A. (2011). Teaching chemistry with spreadsheet. Chemical Education, 22(4), 357-362. https://doi.org/10.1016/s0187-893x(18)30157-5
16. Raviolo, A. (2012). Re-creating simulations with the spreadsheet. Chemical Education, 23(1), 11–16. https://doi.org/10.1016/s0187-893x(17)30092-7
17. Raviolo, A., Alvarez, M., & Aguilar, A. (2011). The spreadsheet in the teaching of Physics: re-creating simulations. Journal of Physics Education, 24(1), 97–107. Retrieved from https://revistas.unc.edu.ar/index.php/revistaEF/article/view/8162
18. Razzak, A., & Uddin, Z. (2023). GUI of vector analysis on spreadsheets for students and teachers. Revista Mexicana de Física E, 20(1), 1-3. https://doi.org/10.31349/revmexfise.20.010208
19. Sabarudiin, N., Pratidhina, E., Kuswanto, H., & Alkiram, S. (2024). Visualization of non-linear continuous wave dispersion effects on fiber grating with spreadsheets in online learning. Revista Mexicana de Física E, 21(2), 1-5. https://doi.org/10.31349/revmexfise.21.020203
20. Suárez, A., & Tornaría, A. F. (2019). Analysis of a nonlinear oscillator using the Euler method on a spreadsheet. Revista Mexicana de Física E, 65(2 Jul-Dec), 200-205. https://doi.org/10.31349/revmexfise.65.200
21. Uddin, Z., Razzak, A., Ahmed, F., & Iqbal, M. (2023). Teaching physics using Microsoft Excel-II. Physics Education, 58(5). https://doi.org/10.1088/1361-6552/acdbb1
22. Watson, C., Templet, T., Leigh, G., Broussard, L., & Gillis, L. (2023). Student and faculty perceptions of effectiveness of online teaching modalities. Nurse Education Today, 120, 105651. https://doi.org/10.1016/j.nedt.2022.105651